International Journal of Fracture **46**: 141–158, 1990.

Three-dimensional stress intensity factor analysis of a surface crack in a high-speed bearing

ROBERTO BALLARINI and YINGCHUN HSU
Department of Civil Engineering, Case Western Reserve University, Cleveland, Ohio 44106, USA

Received 23 June 1989; accepted 12 September 1989

Abstract. The boundary element method is applied to calculate the stress intensity factors of a surface crack in the rotating inner raceway of a high-speed roller bearing. The three-dimensional model consists of an axially stressed surface cracked plate subjected to a moving Hertzian contact loading. A multi-domain formulation and singular crack-tip elements were employed to calculate the stress intensity factors accurately and efficiently for a wide range of configuration parameters. The results can provide the basis for crack growth calculations and fatigue life predictions of high performance rolling element bearings that are used in aircraft engines.

1. Introduction

Current development of very high performance rolling element bearings for aircraft engines has aroused concern about the growth of surface cracks in the inner bearing race. At high DN values (where D is the diameter of the bearing bore in millimeters, and N is the shaft speed in RPM) these cracks may propagate and ultimately lead to catastrophic failure of the bearing and the engine. Raceway fracture is therefore a totally unacceptable failure mechanism. An accurate crack stress analysis is essential in order to make a reliable prediction of the fatigue life of a surface cracked component. However, due to the complexities of the nature of the surface crack problem, closed form solutions are not possible, and a numerical or an experimental approach must be used to determine the stress intensity factors for surface cracks. The Boundary Element Method (BEM) is an efficient and accurate tool for fracture mechanics analyses if singular elements and multi-domain modelling are employed. Therefore this method was employed in the current research for calculating the stress intensity factors along the crack front of a surface crack subjected to various loading conditions.

Several factors will affect the growth of surface cracks in a rotational bearing subjected to a rolling contact load. These include the shape and inclination of the crack, the tensile hoop stress due to rotation and shrink fit, the moving Hertzian load, the pressure of the lubricant seeping into the crack, the shear stress on the raceway surface due to the sliding contact, and friction along the crack surfaces. A significant amount of research has been conducted aimed at gaining a better understanding of the effects of each of these factors. While the surface crack is a three-dimensional problem, most of the analyses which appear in the literature are two-dimensional. These include the work of Way [1], which considers the effects of the lubricant, Fleming and Suh [2, 3], which considers the effects of contact surface friction, Rosenfield [4], which considers the effects of crack surface friction, and Clark [5], which considers the effects of tensile hoop stresses. A recent paper by Mendelson and Ghosn

[6] presents the results of a thorough BEM analysis of a crack propagating through a high speed bearing. The two-dimensional analysis employs a modified Forman-type crack propagation law to predict the fatigue life of a typical bearing subjected to tensile hoop stress superimposed on a cyclic Hertzian contact loading. They compared their results with experimentally observed fatigue lives and found their predictions to be conservative by a factor of 12. However, they demonstrated that the crack driving force in such problems is the alternating mixed-mode loading which occurs with each passage of the roller. Based on these results, the present research was aimed at quantifying the three-dimensional effects. The mechanical model proposed in this paper neglects some of the factors mentioned previously. It is assumed that lubrication renders surface sliding friction negligible. The pressure on the crack surfaces which may arise from the lubricant seeping into the crack is ignored since the Hertzian load moves past the crack very quickly and thus the viscosity, compressibility and inertia of the oil will prevent significant pressurization [7]. Moreover, since the radius of the Hertzian contact area is smaller than the assumed initial surface length of the crack, oil is allowed to squeeze out of the crack. The friction between the crack surfaces is neglected, since it tends to increase the resistance to crack growth. Including this friction in the model is straightforward, but was not done in the present research in order to save computer time. Thus the only factors assumed to be important to the present model are the mechanical loads which arise from the Hertzian contact, rotation, and shrink fit.

2. Formulation

2.1. Numerical solution of the boundary integral equations

Because of space limitations, a detailed description of the numerical techniques and algorithms that were employed to solve the discretized form of the integral equations cannot be presented here. However, a brief description of some of the techniques which lead to accurate and efficient modelling of crack problems is warranted.

The BEM relies on the singular solution of the Navier equations due to a point load and Betti's reciprocal theorem. The integral equations have the form

$$C_{ij}(P)u_j + \int_\Gamma T_{ij}(P, Q)u_j(Q)\,\mathrm{d}\Gamma(Q) = \int_\Gamma U_{ij}(P, Q)t_j(Q)\,\mathrm{d}\Gamma(Q), \tag{1}$$

where u_j and t_j are the displacement and traction vectors respectively, P is the source point indicating the location at which the force acts, Q is the field point denoting the actual boundary point, and r is the distance between them. The integrals are Cauchy principal value integrals and $C_{ij}(P)$ is a field of constants which depends on the smoothness of the boundary at P. The procedures for obtaining a numerical solution to (1) starts out with a discretization of the boundary Γ into isoparametric surface elements. Within each element, the unknown functions may be assumed either constant or to vary linearly, quadratically, etc. In the present analysis, quadratic variations were employed. A Gaussian quadrature scheme can then be applied to evalulate the integrals. For the case when point P is not on the element which is being integrated, the quadrature is straightforward. However, when point P is one of the nodes of the element under integration, direct application of Gaussian quadrature will lead to inaccurate results because of the $1/r$ and $1/r^2$ singularities in the tensors U_{ij} and T_{ij}. Special treatment of the singularities must be used to obtain accurate solutions. The method

employed in the present research follows the work of Rizzo and Shippy [8]. The elements are divided into triangles and the integration is carried out after the coordinates are transformed into a local polar coordinate system. The transformation leads to an "r" term in the numerator which cancels the "r" term in the denominator. Gaussian quadrature can then be applied to the polar coordinate system. However the $1/r^2$ singularity is not eliminated since the extra "r" term can only reduce the singularity to $1/r$. To eliminate this remaining singularity, the integral equations and the shape functions are manipulated in such a way that when the point P is one of the nodes of the element being integrated, the terms containing $1/r^2$ cancel. The details of the manipulations can be found in [9]. Using these procedures, all the singularities are eliminated and Gaussian quadrature can be used to reduce the integral equation to a system of linear algebraic equations in terms of the (discrete) unknown nodal tractions and displacements along the boundary of the body. Before the system of equations can be solved, the relevant boundary conditions must be imposed. That is, at each point along the boundary either the traction vector or displacement vector is prescribed.

2.2. Subregion technique

In linear elastic fracture mechanics, crack surfaces are modelled as infinitesimally thin cuts. Therefore two material points on the surface of the body are allowed to occupy the same geometrical point. However, the boundary integral equation is a relation where kernel functions include the terms $1/r$, $1/r^2$, thus this is not allowed. There are two ways a crack can be modelled using BEM. One can either separate the crack surfaces by a finite distance *a priori*, or partition the boundary into subregions and apply the compatibility and equilibrium conditions. Since the first method leads to inaccurate results, the second method is chosen for the present study. Consider for simplicity the case (Fig. 1) where the body

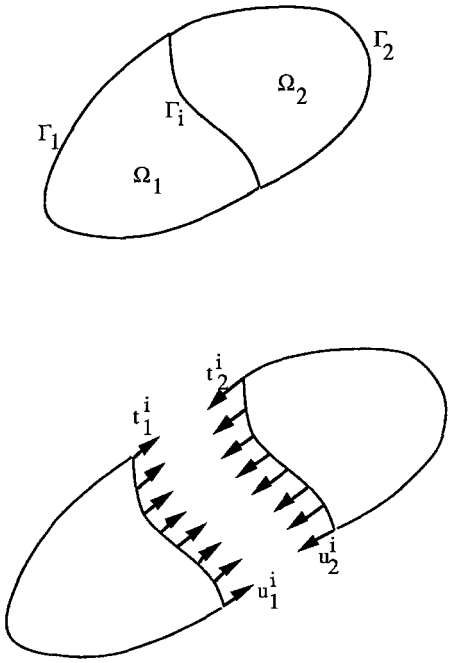

Fig. 1. Partitioning of domain.

occupying domain Ω and bounded by surface $\Gamma = \Gamma_1 \cup \Gamma_2$ is partitioned into domains Ω_1 and Ω_1 which are bounded by surfaces $\Gamma_1 \cup \Gamma_i$ and $\Gamma_2 \cup \Gamma_i$, where Γ_i is the interface which joins the two subregions. The multi-domain technique consists of transforming the integral equations to algebraic equations for each subregion, as described in the previous section, and requiring continuity of displacements as well as equilibrium along Γ_i, i.e.

$$\begin{aligned} t_i^1 &= -t_i^2 = t_i, \\ u_i^1 &= u_i^2 = u_i, \end{aligned} \tag{2}$$

where t_i and u_i are the traction and displacement vectors along Γ_i, respectively. The details of the algorithms used to solve the equations can be recovered in [9].

2.3. Singular elements

The variation of any function in an isoparametric element is polynomial. The degree of the polynomial depends on the number and arrangement of the nodes. Therefore, if a quadratic surface element is used in the vicinity of a crack, the distributions of stresses and displacements in the elements will at most have quadratic variations. The use of these elements would require a very fine mesh to capture the $\sqrt{r}$ variation in displacements and $1/\sqrt{r}$ variation in stresses predicted by linear elasticity. Fortunately, this problem was solved by Barsoum [10], who modified the quadratic isoparametric elements by relocating appropriate mid-side nodes to the quarter point (Fig. 2). This transformation leads to the proper ($\sqrt{r}$) asymptotic behaviour for the displacements. To capture the $1/\sqrt{r}$ behaviour of the stresses, the shape functions are modified by multiplying the stress approximations by the factor $\sqrt{(L/r)}$, where L is the length of the element. This leads to the correct asymptotic behaviour [9]. The details of the stress intensity factors calibration is given in [9].

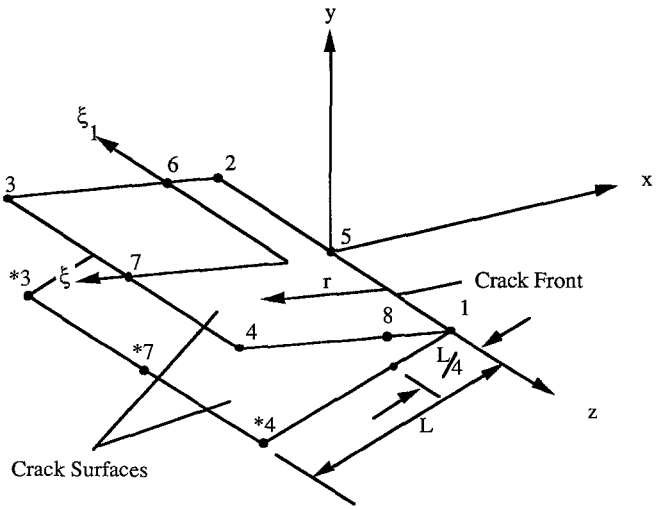

Fig. 2. 8-node quarter point element.

3. Verification problems

Two problems were studied to assess the accuracy and efficiency of the method. The calculations were performed using single precision on a CRAY X-MP. The material properties are as follows: $E = 30\,000$ ksi and $\nu = 0.3$.

3.1. Inclined circular crack under uniform tension

This problem was solved to assess the ability of the method to calculate stress intensity factors for mixed-mode fracture problems. The exact solution to the problem shown in Fig. 3 is [11]

$$K_{\mathrm{I}}^{A} = \left[\frac{2}{\pi}\,\sigma\sqrt{\pi a}\,\sin^2\phi\right], \tag{3}$$

$$K_{\mathrm{II}}^{A} = \left[\frac{4}{\pi(2-\nu)}\,\sigma\sqrt{\pi a}\,\sin\phi\cos\phi\right]\cos\omega, \tag{4}$$

$$K_{\mathrm{III}}^{A} = \left[\frac{4(1-\nu)}{\pi(2-\nu)}\,\sigma\sqrt{\pi a}\,\sin\phi\cos\phi\right]\sin\omega, \tag{5}$$

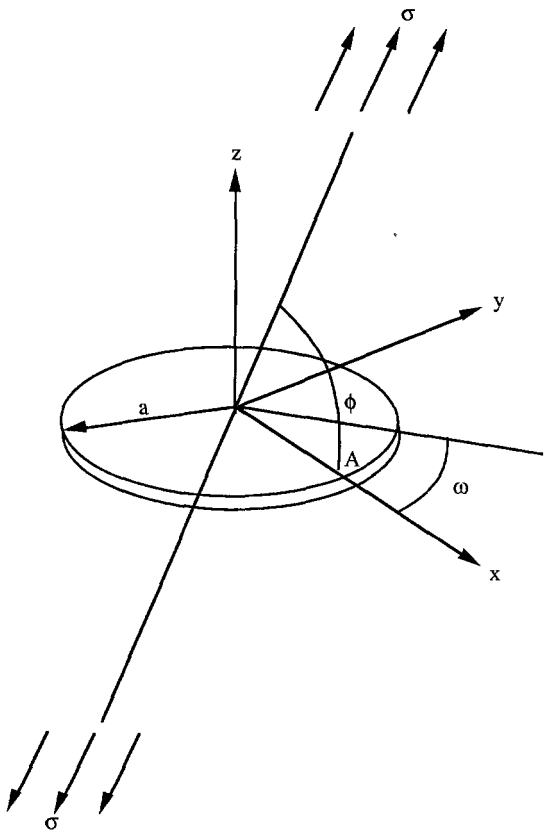

Fig. 3. Inclined buried circular crack.

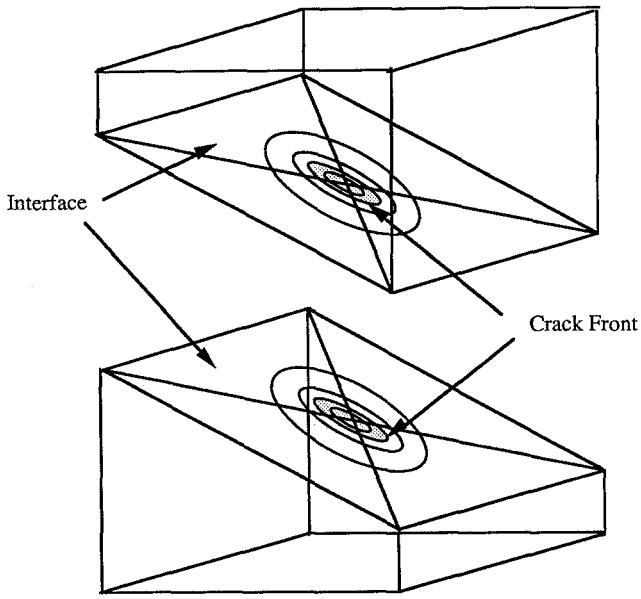

Fig. 4. Double region mesh for inclined buried circular crack.

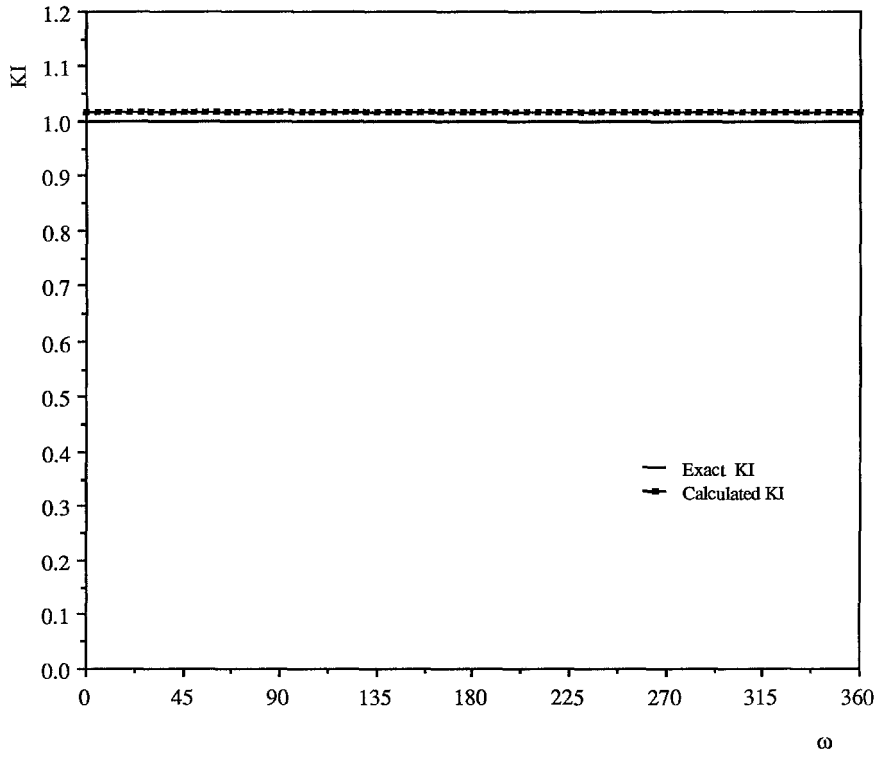

Fig. 5. Comparison of K_I with exact solution for inclined buried circular crack.

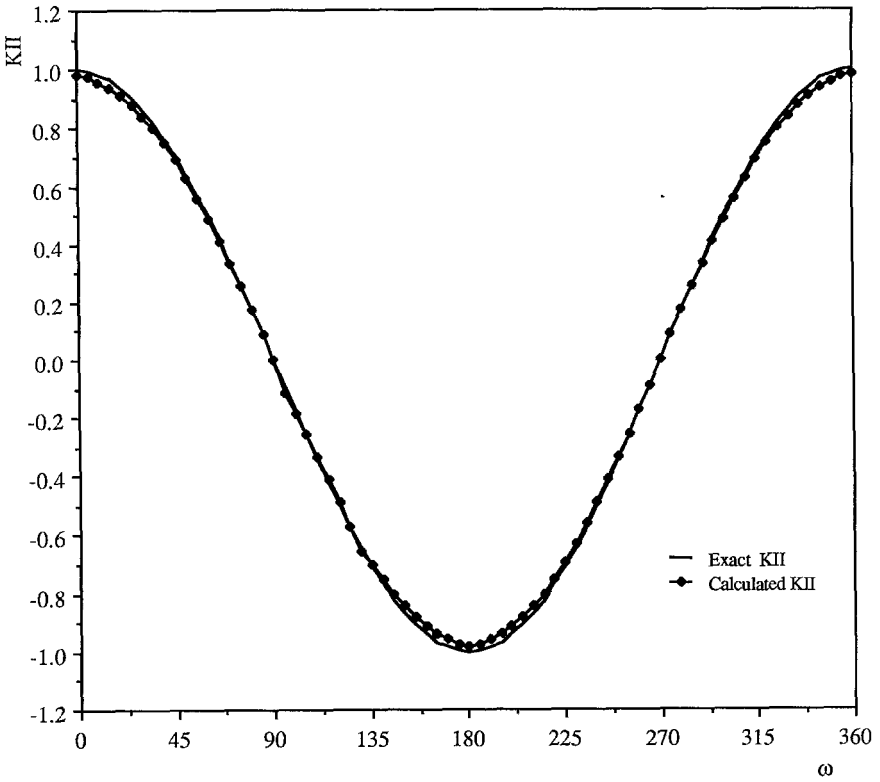

Fig. 6. Comparison of K_{II} with exact solution for inclined buried circular crack.

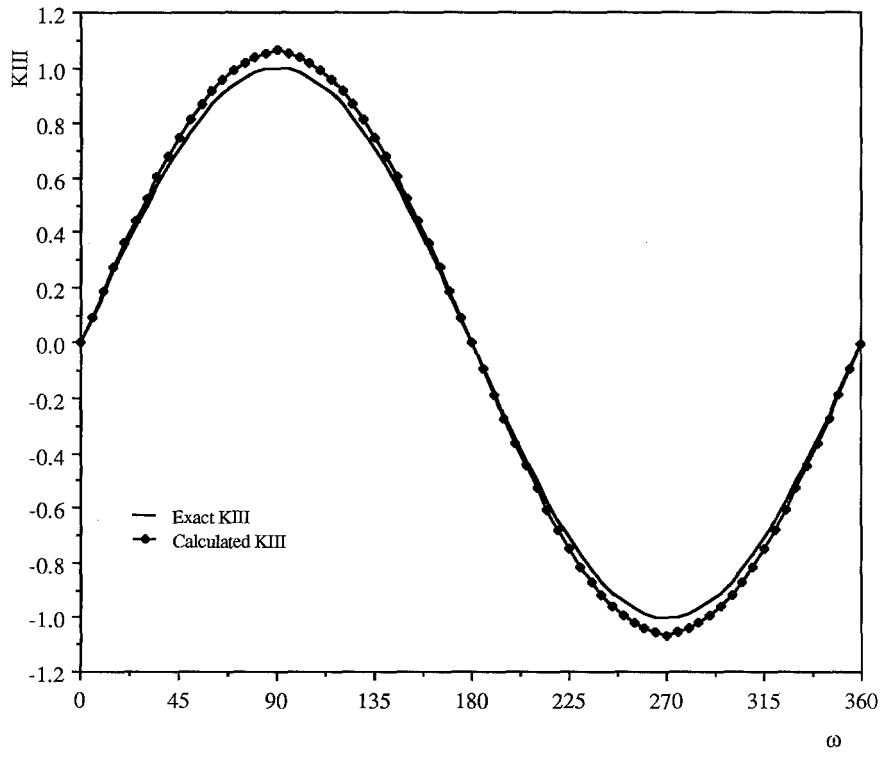

Fig. 7. Comparison of K_{III} with exact solution for inclined buried circular crack.

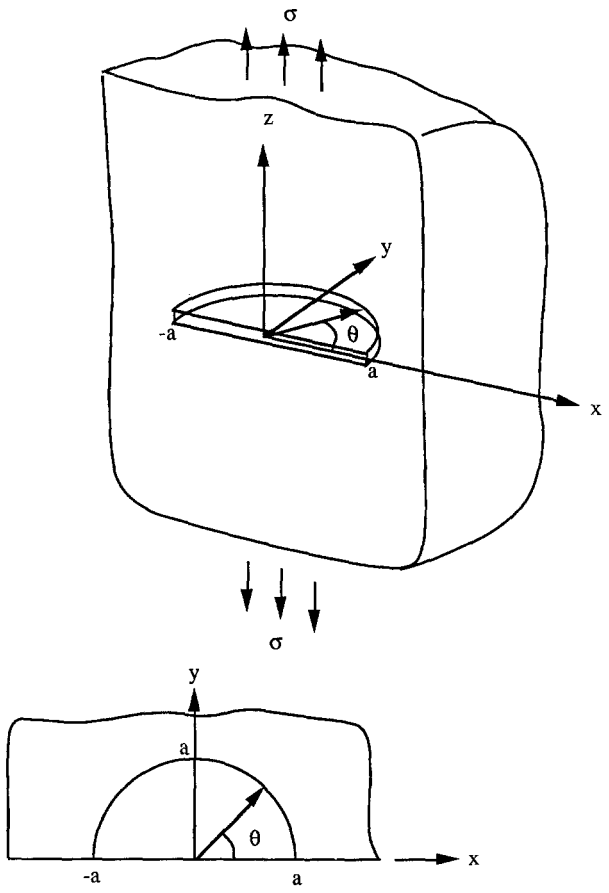

Fig. 8. Semicircular surface crack under tension.

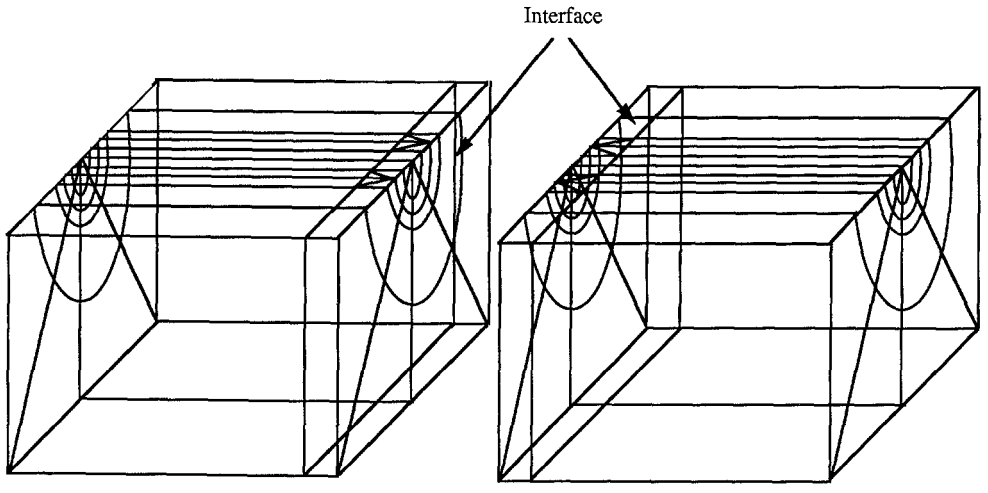

Total number of nodes: 404 (202 for each subregion)
Total number of elements: 144 (72 for each subregion)

Fig. 9. Double region mesh of semicircular surface crack under tension.

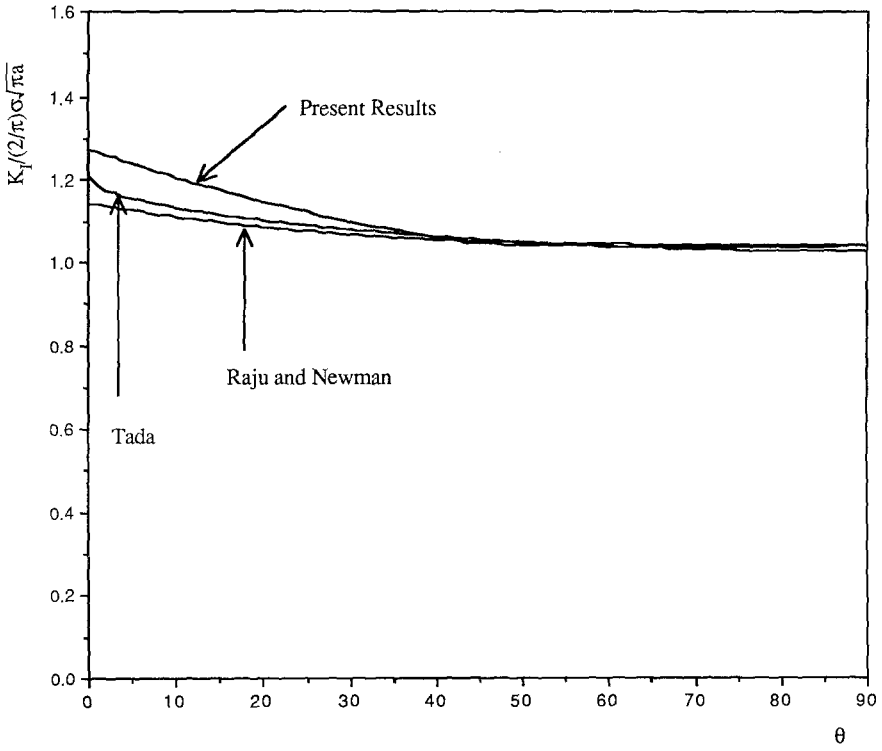

Fig. 10. Comparison of K_I with published solutions for semicircular surface crack.

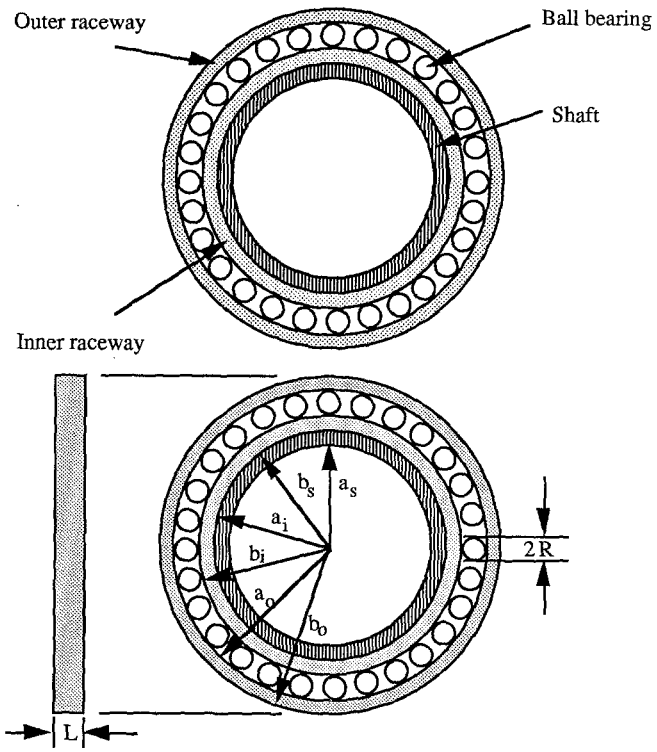

Fig. 11. Geometry of bearing.

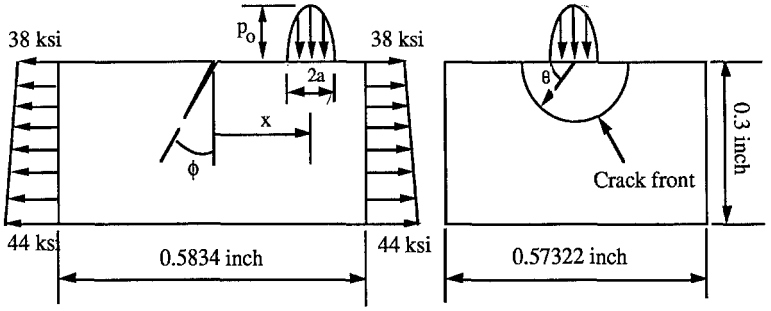

Fig. 12. Model of bearing.

where, as shown in Fig. 3, ϕ is the angle between the direction of the applied stress and the normal to the crack plane and ω is the angle which locates the point A. Because there is no symmetry in this problem, it is necessary to use a double region mesh. The results for the mesh shown in Fig. 4 (the crack is inclined at 30 deg) are presented in Figs. 5–7. The stress intensity factors have been normalized with respect to the quantities in the square brackets in (3) to (5). The errors in K_I^A, K_{II}^A and K_{III}^A are approximately 1.2%, 2.3% and 5.7% respectively. The total CPU time needed to solve the problem is 131 seconds.

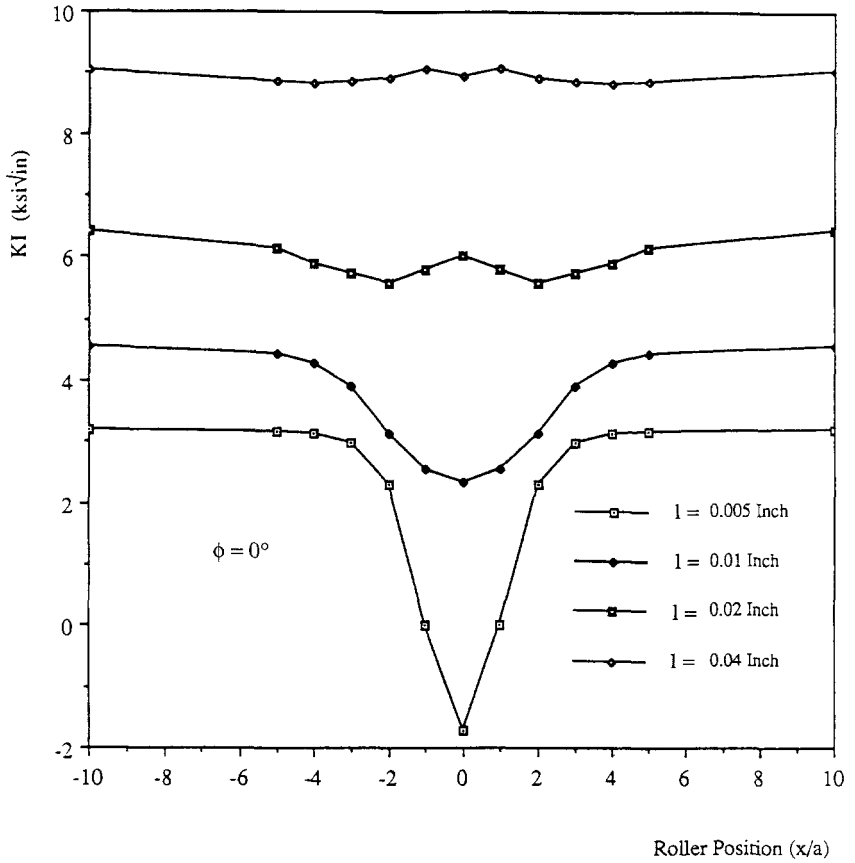

Fig. 13. Variation of K_I at $\theta = 90°$ with roller position and crack length for $\phi = 0°$.

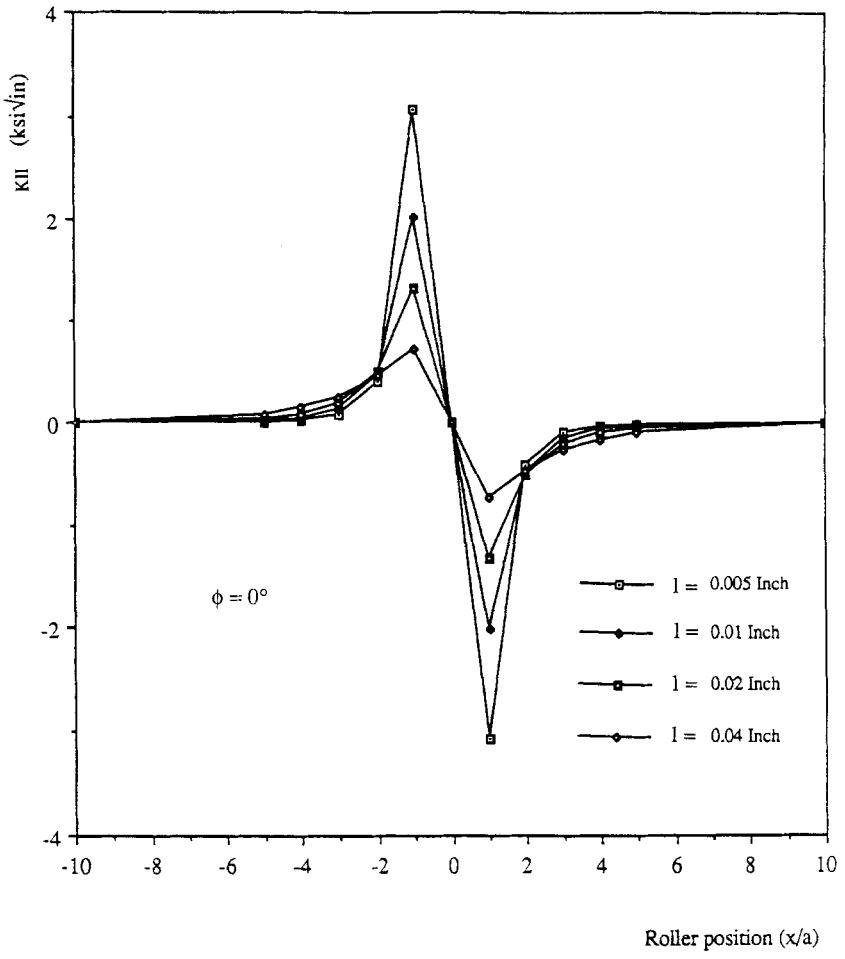

Fig. 14. Variation of K_{II} at $\theta = 90°$ with roller position and crack length for $\phi = 0°$.

Table 1. Dimensions and material properties of typical ball bearing for aircraft engines.

Shaft	Inner radius $a_s = 2.0$ in.
	Outer radius $b_s = 2.30233$ in.
Inner raceway	Inner radius $a_i = 2.3$ in.
	Outer radius $b_i = 2.6$ in.
Outer raceway	Inner radius $a_0 = 3.1$ in.
	Outer radius $b_0 = 3.35$ in.
Bearing length L	0.57322 in.
Ball bearing	Radius $R = 0.25$ in.
No. of ball bearings	28
Shaft speed	25 500 rpm
	$E = 3.0 \times 10^7$ psi
M50 steel material	$\rho = 0.288$ lb/in^3.
properties	$\nu = 0.3$
	$K_{IC} = 18$ ksi$\sqrt{}$in.

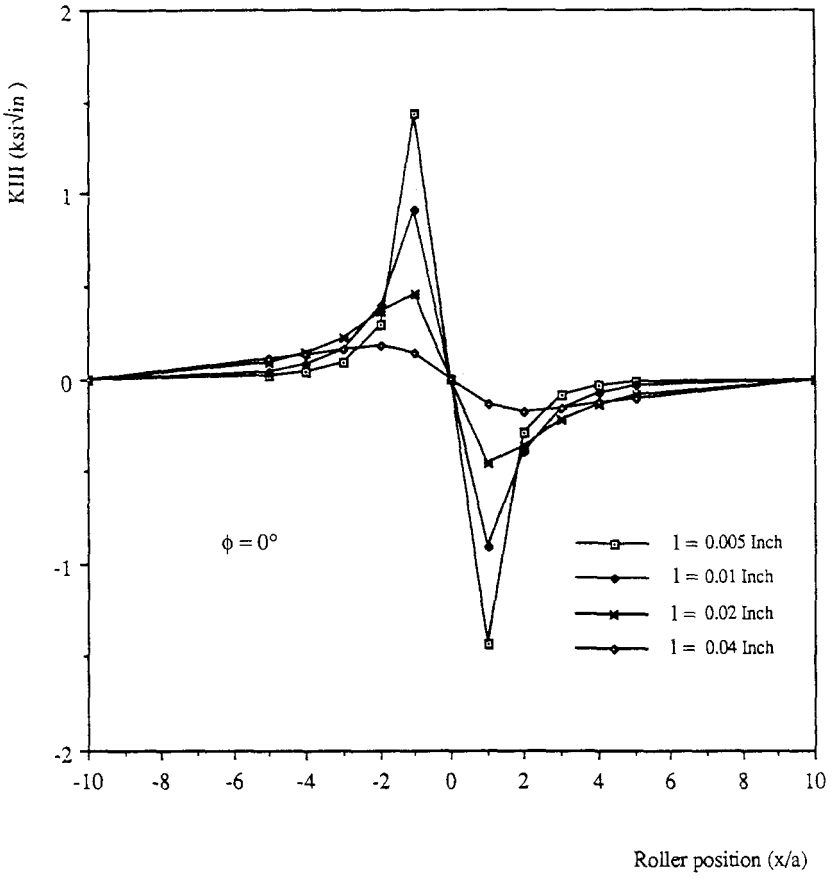

Fig. 15. Variation of K_{III} at $\theta = 45°$ with roller position and crack length for $\phi = 0°$.

3.2. Semi-circular surface crack under uniform tension

This example was solved to check the accuracy of the method for surface crack problems. An exact solution to the problem shown in Fig. 8 does not exist. However, numerical results are available. Tada [11] presents K_I for a semi-circular surface crack in a semi-infinite body subjected to uniform tension as

$$K_I(\theta) = \frac{2}{\pi}\sigma\sqrt{\pi a}F(\theta), \tag{6}$$

where

$$F(\theta) = 1.211 - 0.186\sqrt{\sin\theta} \text{ (for } 10° < \theta < 170°) \tag{7}$$

and θ is measured from the surface as shown in Fig. 8.

Newman and Raju [12] predict

$$K_I(\theta) = \sigma\sqrt{\pi a}F(\theta)/\sqrt{2.464}, \tag{8}$$

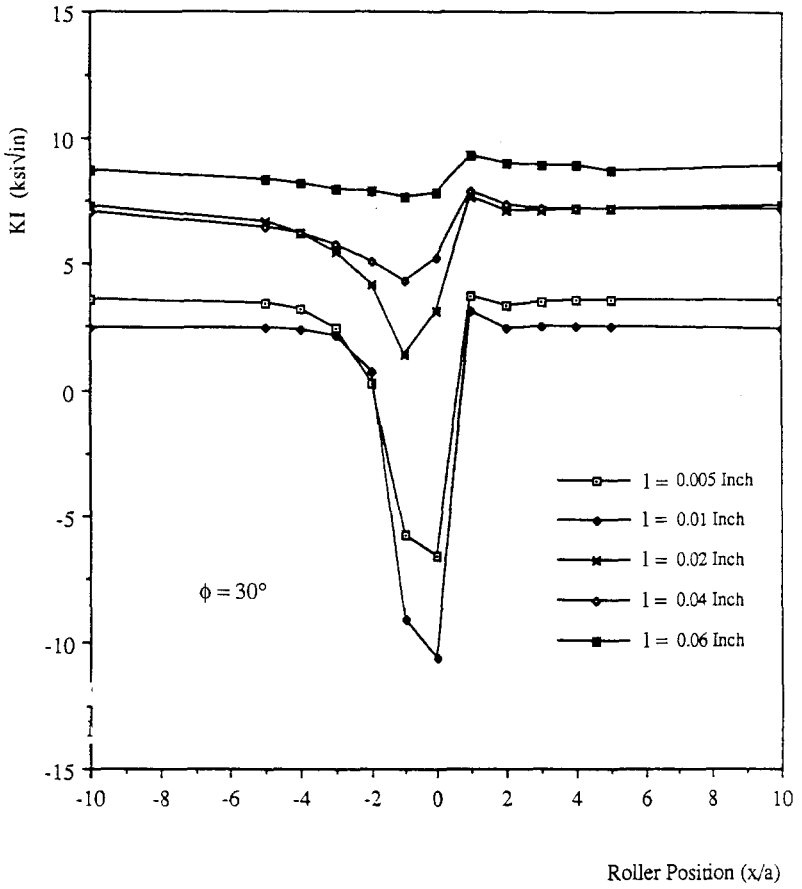

Fig. 16. Variation of K_I at $\theta = 90°$ with roller position and crack length for $\phi = 30°$.

where

$$F(\theta) = 1.04\,[1 + 0.1(1 - \sin\theta)^2]. \tag{9}$$

The double region model shown in Fig. 9 was used to solve the problem. A comparison of our results with those of Tada [11] and Raju [12] is shown in Fig. 10. The maximum difference is approximately 5.7 percent at the point where the crack meets the free surface. This is a result of K_I being calculated assuming plane strain conditions and an inverse square root stress singularity. These assumptions may not be valid at this point.

The excellent results obtained in this verification exercise provide confidence in studying the roller bearing problem.

4. Stress intensity factor analysis

This section presents the results of a quasi-static stress intensity factor analysis of the inner raceway of the bearing shown in Fig. 11. The dimensions and properties of the components are listed in Table 1. The bearing consists of 28 ball rollers. To simulate the passage of each

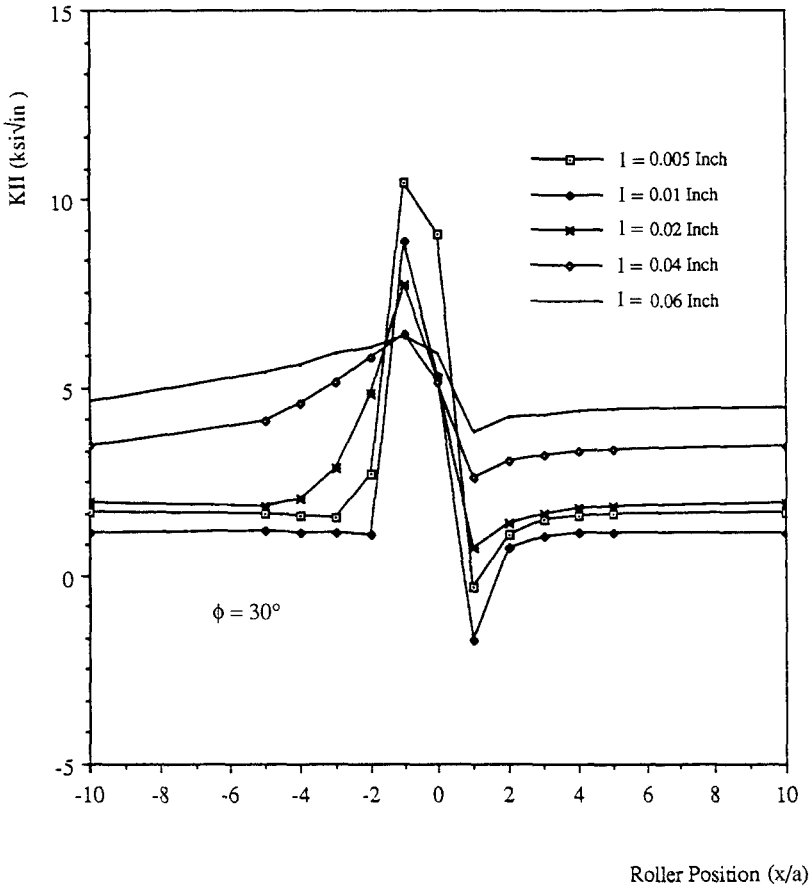

Fig. 17. Variation of K_{II} at $\theta = 90°$ with roller position and crack length for $\phi = 30°$.

ball 1/28th of the inner raceway is modelled. Since the radius of the inner raceway is large compared to the other dimensions, the curvature is neglected and the structure is modelled as a surface cracked plate with flat surfaces, as shown in Fig. 12. The surface crack is assumed to be semi-circular with radius 1, and may be inclined at an angle ϕ from the vertical. The hoop stresses shown in Fig. 12 arise from rotation and shrink fit. The details of the calculations are given in [9]. It was shown in [13] that the interaction between a surface crack and an indentor will not, at least for two-dimensional problems, significantly alter the contact stress distribution. Thus, the ball bearings are replaced with a circular distribution given by

$$p = p_0\left(1 - \frac{x^2}{a^2} - \frac{y^2}{a^2}\right)^{1/2}, \tag{10}$$

where a is the radius of the circular contact area and p_0 is the maximum intensity, which is given in terms of the total load P by

$$p_0 = \frac{3}{2}\frac{P}{\pi a^2}. \tag{11}$$

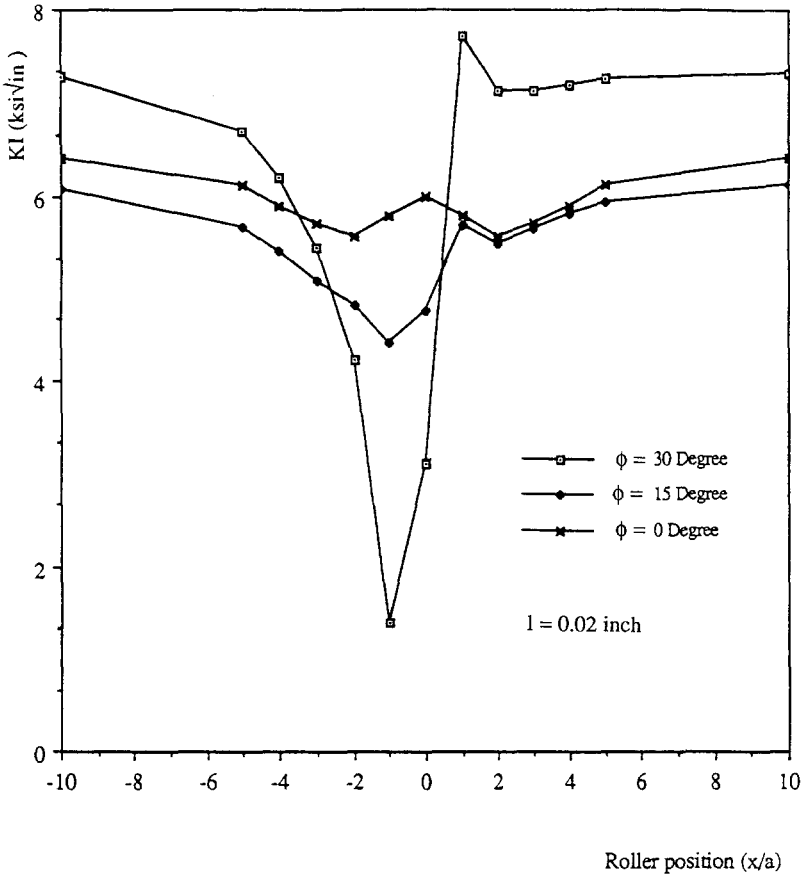

Fig. 18. Variation of K_I at $\theta = 90°$ with polar position and inclination angle for $l = 0.02$ in..

The radius can be calculated from

$$a = \left(\frac{3PR(1 - \nu)^2}{2E}\right)^{1/3}. \tag{12}$$

As discussed in [6], the experimental data indicates that for the bearing considered in the present analysis $p_0 = 285$ ksi. ($a = 0.02574$ in.). Subsequent calculations are based on this value. It should be noted that the depth of the plate is assumed to be large enough so that the distribution of contact stresses remains Hertzian.

The distance x between the centre of the Hertzian distribution and the crack mouth is changed incrementally to simulate the passage of each roller.

The stress intensity factors for this problem vary with position along the crack front (θ). A typical variation of the mode I stress intensity factor at $\theta = 90$ deg with roller position and crack length for a vertical crack ($\phi = 0$ deg) is shown in Fig. 13. When the roller is at distances greater than three times the contact length from the crack mouth, the stress intensity factor is a constant which results from the axial stress. As the roller gets closer, the compressive stresses arising from the Hertzian load decrease the stress intensity factor. When the load is on the crack mouth the stress intensity factors for all but the longest crack become negative, indicating crack closure.

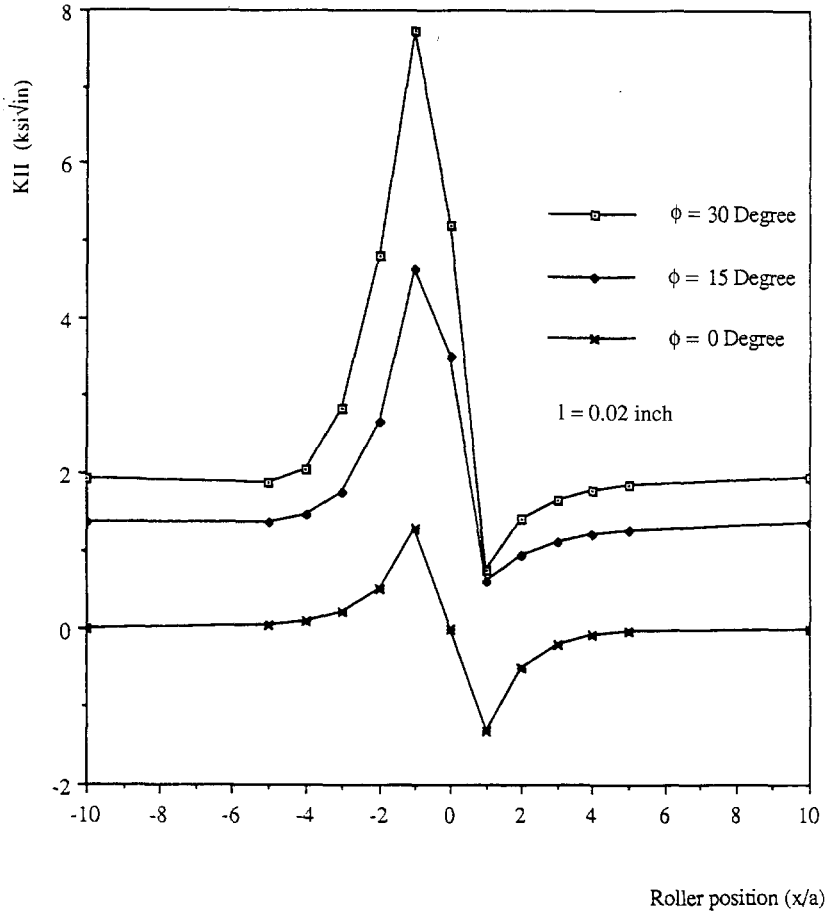

Fig. 19. Variation of K_{II} at $\theta = 90°$ with roller position and inclination angle for $l = 0.02$ in..

The variation of the mode II stress intensity factor for the same loading conditions is shown in Fig. 14. The value of K_{II} is zero when the roller is far from the crack mouth. As the roller approaches the crack, K_{II} starts to increase and reaches a maximum value when the load is on the crack mouth. As the roller crosses to the other side of the crack, K_{II} abruptly changes sign and decreases to a minimum value equal in magnitude to the previous maximum. For small crack this change is very abrupt, but for large cracks the change is more gradual. As pointed out in [6], these abrupt variations in K_I and K_{II} may significantly affect the propagation of short cracks.

Although the results are not presented here, it was observed that the magnitudes and variations of K_I and K_{II} for $\theta = 45$ deg did not differ significantly from $\theta = 90$ deg. However, as shown in Fig. 15, at $\theta = 45$ deg a mode III stress intensity arises. The magnitude of K_{III} is less than K_{II}, but the variations with the location of the Hertzian load are similar.

A comparison of the results for $\phi = 0$ deg obtained in the present analysis with those presented in Mendelson and Ghosn [6] revealed that while the variations of K_I and K_{II} with roller position are similar, the magnitudes of the stress intensity factors differ significantly. For $l = 0.02$ in., the maximum value of K_I from Fig. 13 is approximately 6.4 ksi$\sqrt{\text{in}}$, while

in [6] it is approximately 9 ksi$\sqrt{\text{in}}$. The difference in K_{II} is even greater. From Fig. 14 the maximum value of K_{II} is approximately 1.5 ksi$\sqrt{\text{in}}$ for $l = 0.02$, while in [6] it is approximately 10 ksi$\sqrt{\text{in}}$. These differences are due to the fact that the total load needed to produce the experimentally measured 285 ksi maximum Hertzian stress using a circular contact area is much lower than that needed using a cylindrical contact (27.5 lbs instead 1500 lbs). This may have contributed to the overly conservative predictions of fatigue life in [6].

As pointed out in [6], the experimental results indicate that as the roller passes from left to right, the surface crack propagates at an angle ϕ approximately equal to 30 deg. The simulations were therefore repeated for several values of ϕ. Figures 16 and 17 present the stress intensity factors for cracks inclined at $\phi = 30$ deg for several crack lengths. As the roller passes to the right of the crack mouth, it forces the crack surface to separate, thus increasing K_I. It is observed in these figures that the maximum values of both K_I and K_{II} are significantly higher than those for $\phi = 0$ deg. Figures 18 and 19 show the variation of K_I and K_{II} with respect to ϕ for a crack of length $l = 0.02$ in. These results indicate that the crack will propagate at an angle of 30 deg from the vertical, as observed in the experiments.

5. Conclusions

A preliminary stress intensity factor analysis of a typical high speed bearing was conducted using the boundary element method. The results confirm the conclusions made in [6] that the crack driving force in these types of problems is the alternating mixed-mode loading that occurs with each passage of the roller. However, the results obtained in the present three-dimensional analysis suggest much lower stress intensity factors that those predicted for the same problem using a two-dimensional analysis [6]. This results from the fact that the total Hertzian load needed to produce the experimentally observed maximum contact stress using the three-dimensional model is (27.5 lbs.) significantly lower than that required using two-dimensional analysis (1500 lbs.). Although the stress intensity factor data obtained from the analysis has not been reduced to a form suitable for life prediction, these preliminary results can provide a better understanding of the complex interactions between a surface crack, a moving Hertzian load, and an axial stress.

Acknowledgements

The authors are grateful for suport from NASA Lewis Research Center (Grant NAG3-396). Discussions with John Shannon and Erwin Zaretsky have been helpful.

References

1. S. Way, *Journal of Applied Mechanics* 44 (1935) A49–A58.
2. J.R. Fleming and N.P. Suh, *Wear* 44 (1977) 39–56.
3. J.R. Fleming and N.P. Suh, *Wear* 44 (1977) 57–64.
4. A.R. Rosenfield, *Wear* 61 (1980) 125–132.
5. J.C. Clark, *Journal of Aircraft* 12 (1975) 383–387.
6. A. Mendelson and L.J. Ghosn, *Analysis of Mixed-Mode Crack Propagation Using the Boundary Integral Method*, NASA Contractor Report 179518 (1986).

7. C.A. Foord, C.G. Hingley and A. Cameron, *ASME Journal of Lubrication Technology* 91 (1969) 282–293.
8. F.J. Rizzo and D.J. Shippy, *International Journal for Numerical Methods in Engineering* 11 (1977) 1753–1768.
9. Y. Hsu, "Three-Dimensional Analysis of Surface Crack-Hertzian Stress Field Interaction", M.S. Thesis, Case Western Reserve University, August 1989.
10. R.S. Barsoum, *International Journal for Numerical Methods in Engineering* 11 (1977) 85–98.
11. H. Tada, P.C. Paris and G.R. Irwin, *The Stress Analysis of Cracks Handbook*, Paris Productions Inc. (1985).
12. J.C. Newman and I.S. Raju, *Analysis of Surface Cracks in Finite Plates Under Tension or Bending Loads*, NASA Technical Paper 1578 (1979).
13. M.D. Bryant, G.R. Miller and L.M. Keer, *Quarterly Journal of Mechanics and Applied Mathematics* 37 (1984) 467–478.